Title: **Mean stress and plasticity effect prediction on notch fatigue and crack growth threshold, combining the theory of critical distances and multiaxial fatigue criteria**

Authors: **M. Benedetti, C. Santus**

DOI Link: https://doi.org/10.1111/ffe.12910

Mean stress and plasticity effect prediction on notch fatigue and crack growth threshold, combining the theory of critical distances and multiaxial fatigue criteria

M. Benedetti[1*], C. Santus[2]

[1]Department of Industrial Engineering, University of Trento, Trento, Italy

[2]Department of Civil and Industrial Engineering, University of Pisa, Italy

*Contacting Author:

Matteo Benedetti

Tel. +390461282457

Fax +390461281977

E-mail: matteo.benedetti@unitn.it

Abstract

In the present work, we propose a robust calibration of some bi-parametric multiaxial fatigue criteria applied in conjunction with the theory of critical distances (TCD). This is based on least-square fitting fatigue data generated using plain and sharp-notched specimens tested at two different load ratios and allows for the estimation of the critical distance according to the point and line method formulation of TCD. It is shown that this combination permits to incorporate the mean stress effect into the fatigue strength calculation, which is not accounted for in the classical formulation of TCD based on the range of the maximum principal stress. It is also shown that for those materials exhibiting a low fatigue-strength-to-yield-stress ratio, such as 7075-T6, satisfactorily accurate predictions are obtained assuming a linear-elastic stress distribution, even at the tip of sharp notches and cracks. Conversely, for any materials characterized by higher values of this ratio, as quenched and tempered 42CrMo4, it is recommended to consider the stabilized elastic-plastic stress/strain distribution, also for plain and blunt-notched samples and even in the high cycle fatigue regime still with the application of the TCD.

Keywords

Multiaxial fatigue criterion; theory of critical distances; mean stress effect; notch fatigue; crack growth threshold

Nomenclature

a	amplitude
b	fatigue strength exponent (Eq. (3a))
c	fatigue ductility exponent (Eq. (3b))
d	diametral

E	Young's modulus
el	elastic
H'	Ramberg–Osgood coefficient (Eq. (4))
HCF	high cycle fatigue
L, L'	critical distance lengths according to LM and PM
L_{th}	threshold derived critical distance length
LCF	low cycle fatigue
LM	line method
m	mean
max	maximum
n'	Ramberg–Osgood exponent (Eq. (4))
N_f	number of cycles to failure
pl	plastic
PM	point method
QT	quenched and tempered
R	notch root radius
R	load ratio
TCD	theory of critical distances
α, β	material parameters of a fatigue criterion
ε	normal strain
ε'_f	fatigue ductility coefficient (Eq. (3b))
γ	shear strain
ΔK_{th}	crack threshold SIF range
$\Delta\sigma_{\mathrm{fl}}$	plain fatigue limit range
ν	Poisson's ratio
σ	normal stress
σ'_f	fatigue strength coefficient (Eq. (3a))
σ_n	normal stress acting on a generic material plane
σ_{VM}	Von Mises equivalent stress
σ_{YS}	yield stress
σ'_{YS}	cyclic yield stress
τ	shear stress

Introduction

A robust notch fatigue assessment is of paramount importance for the structural integrity prognosis of most machine elements. It is in fact universally accepted by the scientific community that the fatigue response of metallic materials in the presence of stress gradients, such those produced by geometrical discontinuities

(holes, grooves, shoulders, weld beads, etc.), residual stresses (shot peening, welding, etc.), and contact between parts (e.g. turbine disc and blades), is not so much dictated by the peak (or hot spot) stress as by the average stress acting on a material's characteristic structural volume. Peterson[1] and Neuber[2] were the first to understand the capability, quantified as notch fatigue sensitivity, of most metallic materials to accommodate local stress peaks under time-varying loading conditions. Their work paved the way for the main concept underpinning the Theory of Critical Distances (TCD): *the critical condition in a notched or cracked member is achieved when a suitable stress component evaluated at a certain critical distance, or averaged over a domain of a certain critical size, equals a stress value representative of the fatigue failure in a smooth part.* In the 90's of the past century, Taylor[3] and Susmel[4] provided this theory with a sound theoretical framework. Initially, the TCD was formalized in the context of the following assumptions: (i) the notch stress field is linear-elastic; (ii) the fatigue damage phenomenon is controlled by the maximum principal stress range; (iii) the critical distance length L is a material characteristic, which is a function of the load ratio R only and is independent of the notch geometry; (iv) the fatigue calculation is conducted in the high-cycle fatigue (HCF) regime, usually assuming the existence of the material fatigue limit. Taking advantage of the notch-crack analogy necessary to render the TCD insensitive to the notch sharpness, the critical distance can be calculated from the threshold Stress Intensity Factor (SIF) range ΔK_{th} and the full range of the plain specimen fatigue limit $\Delta\sigma_{\mathrm{fl}}$, both obtained at the same load ratio:

$$L_{th} = \frac{1}{\pi}\left(\frac{\Delta K_{th}}{\Delta\sigma_{fl}}\right)^2 \tag{1}$$

where the subscript "th" indicates that L is inferred from ΔK_{th}. When the TCD is formulated in terms of the Point Method (PM), the component is regarded to be in the fatigue limit condition when the maximum principal stress range evaluated at a point located at a distance $L/2$ from the notch root equals the plain fatigue limit, as schematically illustrated by Fig. 1. Conversely, the Line Method (LM) averages the maximum principal stress range along the notch bisector over a length $2L$. Other averaging domains of higher geometrical complexity[5,6] have been proposed in the past, yet receiving much lesser attention than PM and LM, especially because of their complicated implementation.

Despite providing satisfactory fatigue predictions in a wide variety of situations[7-9], this conceptual framework of the TCD suffers from some limitations and drawbacks, which stimulated the scientific community to attempt further improvements:

1) In general, only under uniaxial loading the fatigue damage is controlled by the maximum principal stress range. Under multiaxial conditions, more sophisticated fatigue criteria must be applied, based either on stress tensor invariants (J2), which can be easily converted into the von Mises stress, or Critical Plane (CP) approaches[10]. Susmel and Taylor[11] observed that, in order to preserve the crack-notch analogy, only CP based multiaxial fatigue criteria can be applied in conjunction with TCD, even though this is possible only under the undemonstrated condition that the same value of L_{th} expressed by Eq. (1) is obtained when the mode I is replaced by mode III crack growth threshold and the plain uniaxial is substituted by the plain torsional fatigue limit. After this pioneering work, the

TCD has been applied in combination with CP based fatigue criteria (Modified Wöhler Curve Method (MWCM)[12], Carpinteri[13], Fatemi-Socie[14]) to many multiaxial fatigue scenarios, including weld joints[15], fretting fatigue[16], variable amplitude loading[17]. In the vast majority of papers, the TCD is applied in terms of PM, as this, in contrast to the averaging operation done by LM, preserves the tensor notation of the stress field necessary for the CP definition. The main motivation in favour of combining TCD with CP criteria is the possibility of estimating the fatigue damage on material planes close to the ones on which initiation and initial growth are expected to occur[18], even though the experimental investigations done in [19] attest some discrepancies between predicted and measured crack planes. Indeed, CP approaches postulates the crack initiation to occur on or near the plane of maximum shear stress amplitude, while some experiments indicate prevalent mode I crack propagation also in the early growth stages from the notch tip[19].

2) The application of TCD in concert with a multiaxial fatigue criterion helps to overcome another limitation of the original formulation of TCD, related to the assumption that any point of the notched geometry shall experience the same stress ratio R. This condition is however violated in many situations of practical interest, for instance in the presence of a residual stress field (superimposed to the mean external stresses), which is self-equilibrated and therefore non-uniformly distributed in the body, or due to any elastic-plastic redistribution of the notch stress field. The issue of a point-to-point variation of the load ratio and hence of the material characteristic length is in general addressed by estimating the critical distance value under zero mean stress condition[4] and using a multiaxial fatigue criterion to account for the mean stress effect[20]. This is incorporated into CP based criteria in the form of the maximum normal stress acting on the CP, while J2 methods consider the hydrostatic stress component[21].
3) An issue related to the threshold-based definition of the critical distance L_{th} according to Eq. (1) is that it precludes the TCD from being extended to the medium-cycle fatigue regime. In fact, defining a fracture mechanics parameter representative of the crack growth resistance in this fatigue regime is not straightforward. In a first attempt to overcome this limitation, Susmel and Taylor[22] postulated a gradual transition (expressed as a function of the number of cycles to failure N_f in form of a power-law equation) of L from L_{th} in the high cycle fatigue regime to L_0 under monotonic static failure. Given the difficult application of TCD to predict the static failure of non-brittle structural metals[23], other approaches[24] proposed in the literature suggested determining L vs. N_f on the basis of the S-N curves generated by testing specimens with two different geometries, of which at least one contains a stress concentration feature. Anyway, till now, there is no general consensus if and how L varies with the component lifetime. For instance, Gates and Fatemi[14] assumed L to be identically equal to L_{th} regardless to the fatigue life regime.
4) The assumption of linear-elastic notch stress field is reasonable only in the HCF regime of structural metals with low fatigue-strength-to-yield-stress ratio. Ductile metals, especially in the low-to-medium cycle fatigue regime, undergo in the notch tip neighbourhood plastic deformation leading to

a redistribution of the elastic stress field postulated by TCD. Nevertheless, Susmel and Taylor[7] suggested keeping valid this assumption under small-scale yielding. Other works[18,25] instead proposed to replace the linear-elastic with the elastic-plastic stress distribution, usually estimated through nonlinear Finite Element (FE) analysis. Recently, Gates and Fatemi[26] and Susmel et al.[27] devised elastic-plastic strain-based CP approaches in concert with PM to predict the low-cycle-fatigue (LCF) strength of notched components, wherein the material fatigue strength is determined from multiaxial strain-controlled fatigue tests. Anyway, it is still debated if and to which extent the plastic deformation affects the critical distance L and its dependency upon N_f[22,25].

5) As shown by Gates and Fatemi[14], the TCD predictions are highly sensitive to the value of L_{th} used in either LM or PM formulation. This length, in turn, is particularly affected by the input material parameters used for its definition. While the determination of the plain fatigue limit requires experimental equipment and expertise usually within the reach of any material testing laboratory, an accurate measurement of the threshold may be challenging, especially at negative load ratios. In addition, the threshold is particularly sensitive to the chemical composition, texture, microstructure and experimental procedures[28]. To overcome these drawbacks, the authors[29] recently proposed the use of an optimal V-notched specimen to deduce the material critical distance through an inverse search procedure. In a subsequent paper[30], the authors proved the robustness of the method by comparing the predictions of the TCD obtained using the threshold and the inverse search lengths. In particular, the inverse search length predictions were as accurate as the threshold-based ones when the notch radius is sharper than the component notch detail for which the fatigue strength needs to be predicted.

The method proposed in [29] is based on the original formulation of TCD, viz. on the linear-elastic distribution of the maximum principal stress. The present paper is aimed at extending the use of the optimal notched sample devised in [29] to determine the critical length to be used in conjunction with a multiaxial fatigue criterion. This is useful to establish a critical distance value independent of the load ratio R and to pave the way for future applications of the method to multiaxial fatigue problems. Particular care will be paid in this work to clarify if the critical distance depends on (i) the choice of the multiaxial fatigue criterion (as inferred in their innovative work by Castro et al.[31]), (ii) the PM and LM formulation of TCD, (iii) the fatigue lifetime N_f, (iv) and the elastic-plastic stress/strain distribution ahead of the notch root. For this purpose, the results of fatigue tests carried out in [30] on two structural metallic alloys will be reinterpreted by the light of some well-established multiaxial fatigue criteria. The discussion is complemented by LCF tests carried out to investigate the cyclic strain-stress behaviour to be implemented in elastic-plastic FE analyses and by SEM fractographic observations to shed light on the orientation of the crack during its early propagation stages.

Experimental material and procedures

Details regarding the material and experimental procedures used to generate the fatigue data analysed in the subsequent sections can be found in [30]. In brief, the experimentation was performed on 42CrMo4+QT

(Quenched and Tempered) steel and aeronautical aluminium grade 7075-T6. Their monotonic tensile properties are listed in Table 1. The fatigue characterization was carried out under alternating (load ratio R=−1) and pulsating (R=0.1) axial fatigue on axisymmetric plain and V-notched samples, whose geometry is shown in Fig. 2a and b, respectively. Specifically, notch depth A and V-aperture angle α (see Fig. 1) were devised in [29] to maximize the influence of the notch tip singular stress term and hence to minimize the sensitivity of the critical distance inverse search to the experimental uncertainties. In [30] notched samples of different severities were used and it was found that the *sharp* notch configuration (notch root radius R=0.2 mm) yielded much more accurate critical distance estimation and hence fatigue calculations than the *blunt* one (notch root radius R=1 mm). The SN curves along with the fit curves are shown in Fig. 3. After failure, the fracture surfaces of some samples are examined using a Scanning Electron Microscope (SEM) FEI Quanta 450 ESEM FEG. The samples are fixed on the plate of the microscope initially perpendicular to the beam line, and then tilted by an angle of 55° to have a perspective view of the surface and estimate the initial crack plane angle with respect to the specimen axis orthogonal plane.

The experimentation was complemented by fatigue crack growth tests in [30], conducted at R=−1 and R=0.1 using C(T) and M(T) specimens, respectively. The outcomes in terms of crack threshold ΔK_{th} and resulting estimation of L_{th} are listed in Table 2.

The results of the cyclic stress-strain tests undertaken in [32, 33] on 7075-T651, an Al-alloy similar to the present one, suggest that the fatigue tests carried out in [30] in the fatigue life regime comprised between 10^5 and 3×10^7 cycles are predominantly in linear-elastic conditions, even in the sharp notched samples, owing to the low fatigue-strength-to-yield-stress ratio displayed by the material.

To investigate the cyclic and LCF behaviour of 42CrMo4+QT steel, a specific experimentation is here conducted on axisymmetric hourglass coupons (illustrated in Fig. 2c) with gage diameter of 6 mm extracted from the same material supply. Specifically, strain controlled fatigue tests are performed according to the standard ASTM E606 using a servo-hydraulic universal testing machine INSTRON 8516, equipped with hydraulic grips, a load cell of 100 kN (nonlinearity ±0.1% of R.O.) and a diametral (transversal) extensometer (nonlinearity ±0.15% of R.O.). Each sample is subjected to strain cycles with constant amplitude, triangular waveform, and constant strain rate of 1×10^{-2} s^{-1}. Fully reversed strain amplitudes (strain ratio R_ε = −1) are applied until final failure at 4 diametral strain amplitudes comprised in the range [0.0008, 0.005]. The diametral (ε_d) is converted into axial strain amplitude (ε_a) according to the following equation, assuming plastic incompressibility:

$$\varepsilon_a = \frac{\sigma_{\max}}{E}(1-2\nu) - 2\varepsilon_d \tag{2}$$

where E is the Young's modulus (reported in Table 1) and ν the Poisson's ratio, taken equal to 0.3[34]. The LCF data are elaborated by dividing the total strain amplitude of the half-life stabilized hysteresis loops into its elastic ($\varepsilon_{a,el}$) and plastic ($\varepsilon_{a,pl}$) components, which are then separately fitted according to the Basquin and Coffin-Manson equations, respectively:

$$\varepsilon_{a,el} = \frac{\sigma'_f}{E}\left(2N_f\right)^b \tag{3a}$$

$$\varepsilon_{a,pl} = \varepsilon'_f\left(2N_f\right)^c \tag{3b}$$

The cyclic and monotonic stress-strain curves have been fitted using the Ramberg-Osgood equation:

$$\varepsilon = \frac{\sigma}{E} + \left(\frac{\sigma}{H'}\right)^{1/n'} \tag{4}$$

and the material parameter *H'* and *n'* are reported in Table 3.

Cyclic and low-cycle fatigue properties

The evolution of the cyclic stress amplitude is shown in Fig. 4a as a function of the number of cycles for all the tested strain amplitudes. It can be noted that the material exhibits severe strain softening for all the explored strain amplitude values. This behaviour is typical of metallic materials with martensitic or bainitic microstructures[35-37]. Stabilized half-life stress-strain hysteresis loops are shown in Fig. 4b. It can be noted that the hysteresis cycles are approximately symmetric with respect to the horizontal (strain) axis only at the highest strain amplitudes, while at the lowest ones the compressive is slightly larger than the tensile stress peak. Apparently, due to the past thermo-mechanical history experienced by the material, the yield surface of the virgin material is not perfectly centred with respect to the principal stress axes and this effect is more pronounced when small plastic strains are applied. A similar behaviour was found in [32] for 7075-T651 Al-alloy, which received a stretching treatment prior to aging.

The results of the LCF tests are summarized in Fig. 4c. The best-fit coefficients of the Basquin and Coffin-Manson equations (Eq. (3)) used to interpolate the experimental data are summarized in Table 3. The results of the load controlled fully reversed HCF tests are reported also in Fig. 4c for comparison. It can be noted that Eq. (3) tends to slightly overestimate the HCF strength of the material. Apparently, the aforementioned asymmetry observed in strain-controlled tests results in a (non-zero) negative mean stress, which is beneficial for the fatigue response of the material.

The half-life hysteresis loops of the LCF tests have been used to determine the cyclic stress-strain curve of the material. The cyclic and monotonic stress-strain curves have been fitted using Eq. (4). The best-fit parameters are listed in Table 3. Figure 4d compares the cyclic stress-strain curve with the monotonic curve. It can be noted that the LCF cyclic curve lies below the monotonic curve; hence the material undergoes moderate cyclic softening, even though extrapolating the cyclic curve at strain levels above 0.015 results in a steeper rising behaviour than the monotonic curve.

The results of the strain-controlled tests are used to calibrate the strain-hardening model of 42CrMo4+QT to be implemented in an elastic-plastic FE analysis of the notch and crack tip stress field. Specifically, the material behaviour is represented through a rate-independent, incremental theory of plasticity based on the Von Mises yield surface model with associated plastic flow rule. The hardening rule is given by the superposition of three Chaboche kinematic hardening sub-models[38]. An optimization procedure, described in detail in [39], has been devised to tune the coefficients of the kinematic sub-models so as to minimize a penalty

function defined as the cumulative absolute deviation of the numerical from the experimental values taken from the stabilized hysteresis loop measured at the largest strain amplitude (corresponding to a total axial strain amplitude ε_a=0.015, and a plastic axial strain amplitude $\varepsilon_{a,pl}$=0.012). This choice is motivated by the fact that this strain amplitude level is comparable with those experienced at the tip of the notched samples investigated in the present paper (see the following discussion) and that, at this strain amplitude, the near-symmetric behavior of the material can be more easily captured by the hardening model than that at the lowest strain levels. The best-fit values of the Chaboche parameters are listed in Table 4. Figure 5 illustrates the comparison between the experimental and numerically predicted hysteresis loops represented as a function of the plastic strain component. As expected, the hardening model is in satisfactory agreement with the experimental values at the largest strain amplitudes. However, it is worth noticing that the experimental hysteresis loops do not exhibit, as expected, a vertical ramp just after the load inversion (because of the variation of the only elastic strain component). This discrepancy is due to the fact that the elastic strain component was calculated from the stress considering the Young's modulus *E* estimated from the monotonic tensile tests. However, as attested by several investigations[35,40,41], the cyclic (pseudo-) Young's modulus estimated from the slope of the unloading ramp of cyclic tests differs from the monotonic one and it is a function of the accumulated strain amplitude. Incorporating this effect into a numerical model is considered rather difficult and beyond the scopes of the present paper.

Elastic-plastic stress field

The cyclic material properties of 42CrMo4+QT are used to numerically evaluate the elastic-plastic strain-stress field in the notched and fracture mechanics specimens used in the experimentation undertaken in [30]. The aim thereof is to investigate the effect of the elastic-plastic stress redistribution on the application of some multiaxial fatigue criteria in conjunction with the TCD. Specifically, the notched samples are analysed using an axisymmetric FE model employing four-node isoparametric elements. The mesh in the notch region is refined in a similar fashion to that used in [29] with the purpose of better reproducing stress and strain gradients at the notch tip. The crack tip stress-strain field is analysed using a plane-strain FE model employing eight-node isoparametric elements. The stress singularity at the crack tip is modelled by a radial arrangement of collapsed quarter-point singular elements, as described in detail in [42]. The crack tip element size is chosen to be less than 1/20 of the crack tip plastic zone radius r_p. The global dimension of the model is set so as to reproduce the condition of small scale yielding, wherein r_p is sufficiently small with respect to the region of *K*-dominance. This occurs when the crack length *a* and the uncracked ligament *W-a* satisfy the following requirement [43]:

$$a,(W-a) \geq 2.5\left(\frac{K_I}{\sigma_{YS}}\right)^2 \tag{5}$$

The above-described FE models reproduce the loading history experienced by the samples during testing. Cyclic loading is applied until stabilization of the stress field, which occurs after 50-100 cycles.

Figure 6 illustrates the axial principal stress variation as a function of the distance (measured along the specimen axis of symmetry) from the notch/crack tip. The remote far field axial stress corresponds to the fatigue limit or crack threshold conditions for notched and cracked samples, respectively. Both maximum and minimum values are shown and normalized with respect to the cyclic yield stress σ'_{YS} listed in Table 4. Figure 6a and b refer to the notched samples, while Figure 6c and d illustrate the crack tip stress field. Figure 6a and c shows the alternating, 6b and d the pulsating loading conditions. It can be noted that the plastic deformation produces a redistribution of the notch and crack tip stress field (dashed lines) with respect to the pure elastic solution (solid lines). It is worth noticing that the extension of the plastic zone is larger in the blunt- than in the sharp-notched samples. The elastic-plastic stress cycles remains fully-reversed in the samples tested at R=-1, while the samples tested at R=0.1 undergo a redistribution of the mean stress as well, resulting in a deviation of the local load ratio R from the nominal one. A similar behaviour, not shown here for the sake of brevity, is displayed by the smooth specimens tested at R=0.1, which, also under fatigue limit loading conditions, display an elastic-plastic redistribution of the mean stress value.

Multiaxial fatigue criteria

One of the aims of the present work is to identify the most suitable multiaxial fatigue criterion for predicting, in combination with the TCD, the notch fatigue behavior, even in the presence of an elastic-plastic redistribution of the notch-tip stress field. For this purpose, six multiaxial bi-parametric fatigue criteria, which emerged as the most promising from the literature survey summarized in the Introduction, are considered: two J2 methods devised by Crossland[44] and Sines[45] for proportional loading only, four CP approaches according to Fatemi-Socie[46], Findley[47], Carpinteri[48], and MWCM[49] also suitable for non-proportional (out-of-phase) loading.

The Crossland criterion includes the Von Mises equivalent stress amplitude $\sigma_{VM,a}$, and the maximum hydrostatic pressure p_{max} in a linear equation of the form:

$$\sigma_{VM,a} + \alpha_C \cdot p_{\max} = \beta_C \tag{6}$$

The Sines criterion is very similar, wherein the mean p_m instead of maximum hydrostatic pressure is considered:

$$\sigma_{VM,a} + \alpha_S \cdot p_{\mathrm{m}} = \beta_S \tag{7}$$

The Fatemi-Socie criterion is based on the identification of the critical plane experiencing the maximum range of shear strain γ_a. In addition, it incorporates the mean stress by using the maximum value of normal stress $\sigma_{n,max}$, acting on the plane of maximum shear strain range:

$$\gamma_a \left(1 + \alpha_{FS} \frac{\sigma_{n,\max}}{\sigma_{YS}} \right) = \beta_{FS} \tag{8}$$

where σ_{YS} is the material's yield stress.

Findley proposed to identify the critical plane experiencing the maximum value of a linear combination of both alternating shear stress τ_a and maximum normal stress $\sigma_{n,max}$:

$$\left(\tau_a + \alpha_F \cdot \sigma_{n,\max}\right)_{\max} = \beta_F \tag{9}$$

Carpinteri and Spagnoli[48] observed that the critical plane orientation depends on the material ductility and assumed it to be a function of the material's axial and torsional fatigue strength σ_{AF}, τ_{AF}. Accordingly, the normal of the critical plane normal is inclined by the angle δ with respect to the direction of maximum principal stress expressed as:

$$\delta = \frac{3\pi}{8}\left[1 - \left(\frac{\tau_{AF}}{\sigma_{AF}}\right)^2\right] \tag{10a}$$

The fatigue criterion is a quadratic combination of the shear stress amplitude and the normal maximum stress acting on the critical plane:

$$\sqrt{\sigma^2{}_{n,\max} + \left(\frac{\sigma_{AF}}{\tau_{AF}}\right)^2 \tau_a^2} = \sigma_{AF} \tag{10b}$$

The MWCM is a critical plane-based criterion, which may be written as:

$$\tau_a + \alpha_{MWCM}\frac{\sigma_{n,\max}}{\tau_a} = \beta_{MWCM} \tag{11a}$$

where the shear stress amplitude τ_a and maximum normal stress $\sigma_{n,\max}$ are computed on the critical plane experiencing the largest shear stress amplitude. This fatigue criterion must satisfy the condition:

$$\frac{\sigma_{n,\max}}{\tau_a} \le \frac{\beta_{MWCM}}{2\alpha_{MWCM}} \tag{11b}$$

since, beyond this upper bound, the material failure is expected to be no longer influenced by the shear stress amplitude[49].

The reformulation of the aforementioned fatigue criteria according to LM and PM can be expressed according to Eq. (12a) and (12b):

$$\frac{1}{2L}\int_0^{2L} H_L(x)dx = H_R \tag{12a}$$

$$H_L(L'/2) = H_R \tag{12b}$$

where H_L and H_R indicates the left- and right-hand side of Eqs. (6-11), respectively. H_L depends upon the stress/strain tensor and material's fatigue characteristics and is a function of the Cartesian coordinate x (see Fig. 1), while H_R is a material parameter only, and L and L' are the critical distance lengths according to LM and PM, respectively. It is evident from Eq. (12), that the TCD is here applied considering the stress distribution along the notch bisector (coincident with the x-axis) and not along the path lying on the critical plane of largest shear stress amplitude, as discussed in[14]. The reasonability of this choice will be discussed in the following.

The calibration of the tri-parametric fatigue calculation method expressed by Eq. (12) requires the knowledge of at least three fatigue data generated by testing, at two load ratios, specimens with two distinct

geometries, of which at least one contains a stress concentration feature. To make more robust the determination of the three parameters, we propose in the present work to least-square fit four fatigue data generated from fully-reversed (R=-1) and pulsating (R=0.1) fatigue tests carried out on smooth and sharp-notched specimens, thus taking full advantage of the optimal notch geometry devised in[29]. Specifically, the best-fit parameters are obtained through minimization of the following weighted sum of square residuals:

$$WSSE = \sum_{i=1}^{n} \frac{\left(\sigma_{a,i} - \hat{\sigma}_{a,i}\right)^2}{s_i^2} \tag{13}$$

where $\sigma_{a,i}$ is the i-th experimental fatigue strength (amplitude) for a given fatigue life, $\hat{\sigma}_{a,i}$ is its estimator, s_i is its standard deviation, and n is the number of data (4 in the present case).

Results and discussion

Tables 5 and 6 list the best-fit parameters of the fatigue criteria illustrated in the previous section for 42CrMo4+QT and 7075-T6, respectively. They refer to the materials' fatigue strength data obtained at the fatigue life $N_f = 10^7$ cycles. For the former material, the parameters have been determined considering both linear-elastic and elastic-plastic stress/strain field. It can be noted that the material parameters are quite insensitive to the TCD formulation (either LM or PM), while this latter along with the fatigue criterion greatly influences the critical lengths L and L'. Unexpectedly, they differ from each other by a factor of about 2, as already discussed in [30]. In addition, L and L' considerably deviate from the threshold-derived lengths L_{th} listed in Table 2..This leads to the important conclusions that the critical length requires a specific calibration in relation to the multiaxial criterion used in combination with TCD and that L_{th} may not be an adequate estimator of it. In particular, L_{th} is closer to L' than to L in 42CrMo4+QT and the opposite occurs in 7075-T6. It is also worth noticing that the critical lengths L and L' are only weakly influenced by the elastic-plastic stress redistribution occurring in 42CrMo4+QT, whereas this phenomenon significantly affects the material's parameters of the multiaxial fatigue criterion.

Tables A.1, A.2 and A.3 of the Appendix compare the accuracy of the fatigue criteria in predicting the HCF strength ($N_f = 10^7$ cycles) and crack growth threshold of 42CrMo4+QT, assuming both elastic and elastic-plastic stress/strain field, and 7075-T6, respectively. Predictions are made both (i) for plain and sharp-notched samples used for the parameters calibration and (ii) for blunt-notched and fracture mechanics coupons taken as independent terms of comparison. In this latter case, the plane-strain asymptotic stress field predicted by LEFM[43] or the elastic-plastic crack tip stress distribution shown in Fig. 6c and d are used. When the stress amplitude is not known a priori, as for the independent cases referred to in point (ii), the elastic-plastic stress/strain field is computed via FEM through an iterative procedure, which is stopped when the absolute difference between the stress amplitude assumed for the FEM analysis and that obtained from the solution of Eq. (12) falls below a threshold set at 1%.

It can be noted that in the vast majority of cases the multiaxial criteria yield considerably more accurate fatigue calculation in conjunction with LM rather than with PM, despite the prevailing opinion that the latter method is more suitable to be combined with fatigue criteria. Indeed, PM is less efficient in predicting the

crack growth threshold ΔK_{th}, while it yields predictions of comparable accuracy for the blunt-notched samples. It can be inferred that PM is appropriate only for situations characterized by mild stress gradients. Interestingly, even though the fatigue calculation is here done in the HCF regime, using the elastic-plastic in place of the linear-elastic stress distribution allows for a better accuracy, especially at R=-1. The most accurate predictions are obtained by combining LM with Crossland, Fatemi-Socie or MWCM for 42CrMo4+QT and Crossland, Carpinteri or Findley criterion for 7075-T6. For this latter material, MWCM yields very accurate predictions of plain and notched fatigue strength, but inconsistent estimates (even negative) of the crack growth thresholds due to the violation of the requirement set by Eq. (11b).

The fracture surface SEM observations of the aluminum alloy 7075-T6 and the steel 42CrMo4+QT are shown in Fig. 7 for the load ratio R=0.1 tests, and very similar evidences have been obtained for R=-1, however not reported for brevity. The steel specimen surfaces, Fig. 7 b, d and f are found quite flat with limited roughness, due to the fine-grained metallurgical structure, and orientation merely perpendicular to the specimen axis. On the other hand, the aluminum specimen fracture surfaces, Fig 7 a, c and e showed much more rough fatigue fracture surface and, apart from the plain specimen, a certain initial angle (though quite limited) with respect to the axis perpendicular plane orientation. Despite the fatigue CP multiaxial criteria are all based on shear amplitude stress parameters, Eqs. 6-11, the initial crack orientation on a size on the order of a few tens of microns, i.e. the critical distance length, is not in agreement with the maximum shear stress amplitude orientations, especially for the steel. Indeed, the crack surface is along the V-notch bisector, and this is in agreement with Susmel and Taylor observations[19] where the inclined initiated cracks were only detectable at the grain size. The observed propensity of the crack to extend on the notch symmetry plane supports the approach adopted in this paper to estimate the stress tensor along the x-axis and not along the plane of maximum shear stress amplitude. Besides being in agreement with empirical evidences, this approach is also of easier implementation, as it does not require the research of the plane of maximum τ_a. This is not a straightforward task, as τ_a must be either evaluated at $L'/2$ or averaged over $2L$, thus making Eqs. (12) and (13) a function of the unknown inclination of such plane.

From the above discussion, the J2-based Crossland criterion appears to be the most accurate for both materials, even though applicable only to proportional loading. Same conclusions were drawn in [50], where it was compared with other criteria in predicting the multiaxial fatigue strength of 7075-T6, even in the presence of shot-peening induced residual stresses. It is worth noticing that the Crossland criterion is also particularly suitable to assess the crack growth threshold ΔK_{th} of both materials. Figure 8a and b plots the predictions of this criterion in concert with LM as a function of the load ratio R for 42CrMo4+QT and 7075-T6, respectively, and compares them with experimental data, some of them taken from the literature[51]. It can be noticed that the Crossland criterion captures very well the R-dependency of ΔK_{th} and that, in contrast to 7075-T6, 42CrMo4+QT requires the use of the elastic-plastic in place of linear-elastic crack tip stress field, especially at negative R. The ability of this and some of the remaining criteria, even if to a lesser extent, to calculate ΔK_{th} supports the basic idea of the present work that it is possible to combine LM with some multiaxial fatigue criteria, as the crack-notch analogy at the base of TCD is preserved.

The approach followed so far is then extended to the medium cycle fatigue regime. For this purpose, the parameters of Eq. (12) are calibrated from the plain and the sharp-notch fatigue data taken at different fatigue lives N_f. Figure 9a, b, and c illustrates the variation of L and L' as a function of N_f for 42CrMo4+QT, taking linear-elastic and elastic-plastic stresses, and 7075-T6, respectively. As anticipated before, L and L' differ from each other and strongly depend upon the fatigue criterion used in their combination. In addition, L and L' are a function, in most cases monotonically decreasing, of N_f. This seems in contrast to an earlier report[25], where the authors concluded that the dependency of L upon N_f is nearly eliminated if the linear-elastic notch tip stress field is replaced by the elastic-plastic one.

In conclusion, Figure 10 illustrates the SN curves calculated for the blunt-notched samples. Both LM and PM are used in combination with the four criteria that yielded the most accurate predictions, namely Crossland, Fatemi-Socie, Carpinteri and MWCM. It can be noted that LM and PM yield similar predictions and all four fatigue criteria are in close agreement with the experimental data when dealing with 7075-T6; conversely, their estimates for 42CrMo4+QT differ each other to a greater extent and display higher discrepancy from the experimental data. Here again, (i) the Crossland criterion is the most accurate, (ii) the predictions of all fatigue criteria become more accurate when the elastic-plastic stress distribution is used, even though a general tendency of overestimating the pulsating fatigue strength is evident. This final remark suggests that a deeper comprehension of the material cyclic behaviour underpinning the elastic-plastic stress/strain evolution at the notch tip is necessary and this will be matter of future investigations.

Conclusions

This paper explored the application of several multiaxial fatigue criteria in conjunction with LM and PM formulation of the TCD. For this purpose, experimental data collected in [30] on two structural metallic alloys were used and complemented with LCF tests to characterize the material cyclic stress-strain behaviour.

The followings are the key conclusions that can be drawn from this study:

1) A robust calibration of the parameters of the multiaxial fatigue criterion as well as of the critical length is obtained from least-square fitting the fatigue data taken from the SN curves of plain and sharp-notched coupons tested at two load ratios R. This latter sample geometry was devised in [29] to minimize the sensitivity of the critical distance determination to the uncertainty in the material fatigue characteristics.
2) The LM and PM critical lengths differ from each other and considerably deviate from the threshold-derived length L_{th}. Their value strongly depends on the multiaxial fatigue criterion used in combination with TCD.
3) LM is in general more accurate than PM, especially in the presence of steep stress gradients. Therefore, LM is more suitable than PM for predicting the fatigue strength of components carrying sharp notches or for assessing the crack threshold.

4) For materials exhibiting a low fatigue-strength-to-yield-stress ratio, such as 7075-T6, satisfactorily accurate predictions are obtained assuming a linear-elastic stress distribution, even at the tip of sharp notches and cracks. Conversely, for materials characterized by higher values of this ratio, as 42CrMo4+QT, it is recommended to consider the stabilized elastic-plastic stress/strain distribution, also for plain and blunt-notched samples.
5) The J2-based Crossland criterion yields the most accurate predictions for both material types. Among CP criteria, suitable also for non-proportional loading, Fatemi-Socie and Carpinteri criteria appear to be the most appropriate for 42CrMo4+QT and 7075-T6, respectively, even though satisfactory predictions were obtained with the remaining criteria after the proper calibration of their parameters.

Acknowledgments

This work was supported by the University of Pisa under the "PRA - Progetti di Ricerca di Ateneo" (Institutional Research Grants) - Project No. PRA_2016_36.

Appendix

Tables A.1, A.2 and A.3 list predictions and estimation errors of the HCF strength ($N_f = 10^7$ cycles) and crack growth threshold of 42CrMo4+QT, assuming both elastic and elastic-plastic stress/strain field, and 7075-T6, respectively.

References

[1] Peterson, R. (1995) Notch sensitivity. In: Sines G, Waisman J, editors. Metal fatigue. New York: McGraw Hill, p. 293–306.

[2] Neuber, H. (1961) Theory of notch stresses: principles for exact calculation of strength with reference to structural form and material. 2nd ed. USAEC Office of Technical Information.

[3] Taylor, D. (2007) The theory of critical distances: a new perspective in fracture mechanics. Elsevier Science. ISBN: 9780080444789.

[4] Susmel, L. (2004) A unifying approach to estimate the high-cycle fatigue strength of notched components subjected to both uniaxial and multiaxial cyclic loadings. Fatigue Fract Eng Mater Struct, 27(5), 391–411.

[5] Bellett, D., Taylor, D., Marco, S., Mazzeo, E., Guillois, J. and Pircher T. (2005) The fatigue behaviour of three-dimensional stress concentrations. Int J Fatigue, 27(3), 207–21.

[6] Benedetti, M., Fontanari, V., Allahkarami, M., Hanan, J. and Bandini, M. (2016) On the combination of the critical distance theory with a multiaxial fatigue criterion for predicting the fatigue strength of notched and plain shot-peened parts. Int J Fatigue, 93, 133–47.

[7] Susmel, L. and Taylor, D. (2003) Fatigue design in the presence of stress concentrations. Int J Strain Analysis, 38, 443-452.

[8] Taylor, D., Bologna, P. and Bel Knani, K. (2000) Prediction of fatigue failure location on a component using a critical distance method. Int J Fatigue, 22, 735-742.

[9] Taylor, D. and Wang, G. (2000) The validation of some methods of notch fatigue analysis. Fatigue Fract Eng Mater Struct, 23, 387-394.

[10] Papadopoulos, I.V., Davoli, P., Gorla, C., Filippini, M. and Bernasconi A. (1997) A comparative study of multiaxial high-cycle fatigue criteria for metals. Int J Fatigue, 19, 219-235.

[11] Susmel, L. and Taylor, D. (2006) Can the conventional high- multiaxial fatigue criteria be re-interpreted in terms of the theory of critical distances? Struct Durability Health Monit, SDHM, 2(2), 115–29.

[12] Susmel, L and Taylor, D. (2008) The Modified Wöhler Curve method applied along with the theory of critical distances to estimate finite life of notched components subjected to complex multiaxial loading paths. Fatigue Fract Eng Mater Struct, 31, 1047-1064.

[13] Carpinteri, A., Spagnoli, A., Vantadori, S. and Viappiani, D. (2008) A multiaxial criterion for notch high-cycle fatigue using a critical-point method. Eng Fract Mech, 75, 1864-1874.

[14] Gates, N. and Fatemi, A. (2016) Notch deformation and stress gradient effects in multiaxial fatigue. Theoretical and Applied Fracture Mechanics, 84, 3–25.

[15] Susmel, L. (2008) Modified Wöhler curve method, theory of critical distances and Eurocode 3: a novel engineering procedure to predict the lifetime of steel welded joints subjected to both uniaxial and multiaxial fatigue loading. Int J Fatigue, 30, 888–907.

[16] Vantadori, S., Fortese, G., Ronchei, C. and Scorza, D. (2017) A stress gradient approach for fretting fatigue assessment of metallic structural components. Int J Fatigue, 101, 1-8.

[17] Susmel, L. and Taylor, D. (2012) A critical distance/plane method to estimate finite life of notched components under variable amplitude uniaxial/multiaxial fatigue loading. Int J Fatigue, 38, 7–24.

[18] Gates, N. and Fatemi, A. (2018) Multiaxial variable amplitude fatigue life analysis using the critical plane approach, Part II: Notched specimen experiments and life estimations. Int J Fatigue, 106, 56-69.

[19] Susmel, L. and Taylor, D. (2007) Non-propagating cracks and high-cycle fatigue failures in sharply notched specimens under in-phase Mode I and II loading. Engineering Failure Analysis, 14, 861–876.

[20] Susmel, L., Tovo, R. and Lazzarin, P. (2005) The mean stress effect on the high-cycle fatigue strength from a multiaxial fatigue point of view. Int J Fatigue, 27, 928-943.

[21] Flavenot, J.F. and Skalli, N. (1989) A comparison of multiaxial fatigue criteria incorporating residual stress effects. In: Brown MW, Miller KJ, editors. Biaxial and multiaxial fatigue. London: Mechanical Engineering Publications, p. 437–57.

[22] Susmel, L. and Taylor, D. (2007) A novel formulation of the theory of critical distances to estimate lifetime of notched components in the medium-cycle fatigue regime. Fatigue Fract Engng Mater Struct, 30(7), 567–81.

[23] Cicero, S., Madrazo, V. and Carrascal, I. (2012) On the Point Method load-bearing capacity predictions in Al7075-T651 structural components containing stress risers. Eng Fail Anal, 26, 129–38.

[24] Negru, R., Şerban, D., Marşavina, L. and Magda A. (2016) Lifetime prediction in medium-cycle fatigue regime of notched specimens. Theoret Appl Fract Mech, 84, 140–8.

[25] Susmel, L. and Taylor, D. (2010) An elasto-plastic reformulation of the theory of critical distances to estimate lifetime of notched components failing in the low/medium-cycle fatigue regime. Trans ASME J Eng Mater Technol, 132(2), 021002-1/8.

[26] Gates, N. and Fatemi, A. (2017) On the consideration of normal and shear stress interaction in multiaxial fatigue damage analysis. Int J Fatigue, 100, 322–336.

[27] Susmel, L., Atzori, B., Meneghetti, G. and Taylor, D. (2011) Notch and mean stress effect in fatigue as phenomena of elasto-plastic inherent multiaxiality. Engineering Fracture Mechanics, 78, 1628–1643.

[28] Forth, S., Newman, J., Forman, R. (2003) On generating fatigue crack growth thresholds. Int J Fatigue, 25(1), 9–15.

[29] Santus, C., Taylor, D. and Benedetti, M. (2018) Determination of the fatigue critical distance according to the Line and the Point Methods with rounded V-notched specimen. Int J Fatigue, 106, 208–18.

[30] Santus, C., Taylor, D. and Benedetti, M. (2018) Experimental determination and sensitivity analysis of the fatigue critical distance obtained with rounded V-notched specimens. Int J Fatigue, 113, 113–125.

[31] Castro, F.C., Araujo, J.A. and Zouain, N. (2009) On the application of multiaxial high-cycle fatigue criteria using the theory of critical distances. Engineering Fracture Mechanics, 76, 512–524.

[32] Benedetti, M., Fontanari, V. and Monelli, B. (2010) Numerical simulation of residual stress relaxation in shot peened high-strength aluminum alloys under reverse bending fatigue. J Eng Mater Technol Trans ASME, 132(1), 0110121–9. http://dx.doi. org/10.1115/1.3184083.

[33] Marini, M., Fontanari, V., Bandini, M. and Benedetti, M. (2017) Surface layer modifications of micro-shot-peened Al-7075-T651: experiments and stochastic numerical simulations. Surf Coat Technol, 321, 265–78.

[34] ASM Metals Handbook: Volume 1: Properties and Selection: Irons, Steels, and High-Performance Alloys. ASM International, Materials Park, OH, 2017.

[35] Benedetti, M., Fontanari, V., Barozzi, M., Gabellone, D., Tedesco, M.M. and Plano, S. (2017) Low and high-cycle fatigue properties of an ultrahigh-strength TRIP bainitic steel. Fatigue Fract Eng Mater Struct, 40, 1459–71.

[36] Sauzay, M., Brillet, H., Monnet, I., Mottot, M., Barcelo, F., Fournier, B., et al. (2005) Cyclically induced softening due to low-angle boundary annihilation in a martensitic steel. Mater Sci Eng, A, 400–401, 241–4.

[37] Benedetti, M., Fontanari, V., Bandini, M., Zanini, F. and Carmignato, S. (2018) Low- and high-cycle fatigue resistance of Ti-6Al-4V ELI additively manufactured via selective laser melting: Mean stress and defect sensitivity. Int J Fatigue, 107, 96-109.

[38] J. Lemaitre, J.L. Chaboche, (1990) Mechanics of Solid Materials, Cambridge University Press, Cambridge,.

[39] Bertini, L., Le Bone, L., Santus, C., Chiesi, F. and Tognarelli, L. (2017) High Load Ratio Fatigue Strength and Mean Stress Evolution of Quenched and Tempered 42CrMo4 Steel. Journal of Materials Engineering and Performance, 26(8), 3784–3793.

[40] Yoshida, F., Uemori, T. and Fujiwara, K. (2002) Elastic–plastic behavior of steel sheets under in-plane cyclic tension– compression at large strain. Int. J. Plasticity, 18, 633–659.

[41] Cleveland, R.M. and Ghosh, A.K. (2002) Inelastic effects on springback in metals. Int. J. Plasticity, 18, 769–785

[42] Beghini, M., Benedetti, M., Fontanari, V. and Monelli, D.B. (2010) A general weight function for inclined kinked edge cracks in a semi-plane. Engineering Fracture Mechanics, 77, 1631-1643.

[43] Anderson, T.L. (1995) Fracture mechanics: fundamentals and applications. Boca Raton (FL): CRC Press.

[44] Crossland, B. (1956) Effect of large hydrostatic pressures on the torsional fatigue strength of an alloy steel. In: Proceedings international conference on the fatigue of metals. London: Institution of Mechanical Engineers, p. 138–49.

[45] Sines, G. (1959) Behaviour of metals under complex static and alternating stresses. In: Sines G, Waisman JL, editors. Metal fatigue. New York: McGraw-Hill.

[46] Fatemi, A. and Socie, D.F. (1988) A critical plane approach to multiaxial fatigue damage including out-of-phase loading. Fatigue Fract Eng Mater Struct, 11(3), 149–65.

[47] Findley, W.N. (1959) A theory for the effect of mean stress on fatigue of metals under combined torsion and axial load or bending. J Eng Ind, 81, 301–6.

[48] Carpinteri, A. and Spagnoli, A. (2001) Multiaxial high-cycle fatigue criterion for hard metals. Int J Fatigue, 23, 135–45.

[49] Susmel, L. and Lazzarin, P. (2002) A bi-parametric Wöhler curve for high cycle multiaxial fatigue assessment. Fatigue Fract Engng Mater Struct, 25, 63–78.

[50] Benedetti, M., Fontanari, V., Bandini, M. and Taylor, D. (2014) Multiaxial fatigue resistance of shot peened high- strength aluminium alloys. International Journal of Fatigue, 61, 271–282.

[51] Noorozi, A.H., Glinka, G. and Lambert, S. (2008) Prediction of fatigue crack growth under constant amplitude loading and a single overload based on elasto-plastic crack tip stresses and strains. Engineering Fracture Mechanics, 75, 188–206.

Tables

Table 1. Monotonic tensile properties based on three replicated tests. Standard error corresponds to 1σ uncertainty band.

Material	*E* (GPa)	σ_{YS} (MPa)	σ_{U} (MPa)	*T.E.* (%)
42CrMo4+QT	206±5.9	727±14	875±15	17.6±2.5
Al 7075-T6	70.5±0.2	531±7	595±6	10.0±0.7

E: Young's modulus, σ_{YS}: 0.2% yield stress, σ_U: ultimate tensile strength, *T.E.*: total elongation

Table 2. Fatigue crack growth threshold from experiments conducted in [30]. These permitted the estimation of the threshold derived critical length L_{th}.

Material	Sample geometry	Load ratio R	ΔK_{th} (MPa m$^{0.5}$)	L_{th} (mm)
42CrMo4+QT	M(T)	-1	9.1	0.0433
	C(T)	0.1	7.2	0.0363
Al 7075-T6	M(T)	-1	4.2	0.0555
	C(T)	0.1	2.5	0.0370

Table 3. LCF parameters for 42CrMo4+QT.

Coffin-Manson and Basquin parameters (Eq. (3))				
E (MPa)	σ'_f (MPa)	b	ε'_f	c
206000	4460.3	-0.1633	0.5574	-0.5786

Ramberg-Osgood parameters (Eq. (4))			
Curve	E (MPa)	H' (MPa)	n'
Cyclic	206000	1499.7	0.1438
Monotonic	206000	920.4	0.0359

Table 4. Parameters of the Chaboche kinematic hardening model of 42CrMo4+QT.

C_1 (MPa)	γ_1	C_2 (MPa)	γ_2	C_2 (MPa)	γ_2	σ'_{YS} (MPa)
17096	45	75280	1607	74532	479	361.5

Table 5. Material parameters of the multiaxial fatigue criteria and critical distance lengths for 42CrMo4+QT.

Criterion	Method	Stress field	Parameter 1		Parameter 2		L, L' (mm)
			Symbol	Value	Symbol	Value	
Crossland	LM	elastic	α_C	0.197	β_C (MPa)	388.4	0.0188
		el.-pl.		0.309		419.1	0.0147
	PM	elastic		0.197		388.3	0.0356
		el.-pl.		0.317		420.7	0.0324
Sines	LM	elastic	α_S	0.181	β_S (MPa)	363.9	0.0151
		el.-pl.		0.294		382.6	0.0063
	PM	elastic		0.181		363.9	0.0291
		el.-pl.		0.295		382.7	0.0134
Fatemi-Socie	LM	elastic	α_{FS}	0.453	β_{FS}	2.635×10^{-3}	0.0243
		el.-pl.		0.849		2.387×10^{-3}	0.0210
	PM	elastic		0.452		2.633×10^{-3}	0.0448

		el.-pl.		0.841		2.382×10^{-3}	0.0424
Findley	LM	elastic	α_F	0.081	β_F (MPa)	202.2	0.0241
		el.-pl.		0.116		218.5	0.0182
	PM	elastic		0.080		202.1	0.0446
		el.-pl.		0.119		220.0	0.0389
Carpinteri	LM	elastic	σ_{AF} (MPa)	487.2	τ_{AF} (MPa)	157.0	0.0280
		el.-pl.		447.0		185.9	0.0205
	PM	elastic		489.4		156.3	0.0510
		el.-pl.		446.9		186.0	0.0436
MWCM	LM	elastic	α_{MWCM}	13.12	β_{MWCM} (MPa)	198.4	0.0247
		el.-pl.		20.40		214.6	0.0186
	PM	elastic		13.06		198.3	0.0455
		el.-pl.		20.91		215.6	0.0400

Table 6. Material parameters of the multiaxial fatigue criteria and critical distance lengths for 7075-T6.

Criterion	Method	Parameter 1		Parameter 2		L, L' (mm)
		Symbol	Value	Symbol	Value	
Crossland	LM	α_C	1.392	β_C (MPa)	235.0	0.0672
	PM		1.371		233.7	0.1126
Sines	LM	α_S	0.859	β_S (MPa)	159.9	0.0278
	PM		0.855		159.9	0.0506
Fatemi-Socie	LM	α_{FS}	38.6	β_{FS}	2.128×10^{-2}	0.0477
	PM		34.8		1.962×10^{-2}	0.0826
Findley	LM	α_F	0.373	β_F (MPa)	116.4	0.0448
	PM		0.372		116.2	0.0791
Carpinteri	LM	σ_{AF} (MPa)	160.7	τ_{AF} (MPa)	92.6	0.0503
	PM		160.9		92.4	0.0880
MWCM	LM	α_{MWCM}	16.71	β_{MWCM} (MPa)	96.7	0.0497
	PM		16.44		96.3	0.0861

Table A.1. High-cycle fatigue strength predictions ($N_f=10^7$) for 42CrMo4+QT assuming linear-elastic stress distribution.

Sample	R	Exp.	Method	Crossland		Sines		Fatemi-Socie		Findley		Carpinteri		MWCM	
				Pred.	Err (%)	Pred.	Err (%)	Pred.	Err (%)	Pred.	Err (%)	Pred.	Err (%)	Pred.	Err (%)
Plain	-1	390	LM	364.4	-6.55	363.9	-6.68	373.9	-4.13	373.0	-4.35	360.3	-7.61	370.6	-4.98
			PM	364.4	-6.57	363.9	-6.69	373.8	-4.15	372.9	-4.37	359.8	-7.74	370.4	-5.02
	0.1	337	LM	338.9	0.56	338.9	0.57	338.2	0.36	338.3	0.38	339.4	0.72	338.5	0.44
			PM	338.9	0.56	338.9	0.57	338.2	0.36	338.3	0.39	339.5	0.73	338.5	0.45
Sharp	-1	87.5	LM	88.9	1.55	88.8	1.52	88.8	1.46	88.8	1.45	88.9	1.62	88.7	1.42
			PM	88.9	1.54	88.8	1.52	88.8	1.46	88.8	1.46	88.9	1.60	88.7	1.41

	0.1	80.5	LM	79.2	-1.64	79.2	-1.62	79.3	-1.51	79.3	-1.53	78.8	-2.09	79.3	-1.53
			PM	79.2	-1.64	79.2	-1.62	79.3	-1.52	79.3	-1.53	78.8	-2.10	79.3	-1.54
Blunt	-1	162.7	LM	146.4	-10.01	149.0	-8.42	140.1	-13.88	139.9	-14.04	136.5	-16.08	139.2	-14.46
			PM	146.1	-10.20	148.8	-8.54	139.5	-14.23	139.3	-14.39	135.7	-16.63	138.6	-14.84
	0.1	119.2	LM	132.1	10.83	134.4	12.77	126.4	6.02	126.4	6.04	127.1	6.60	126.5	6.14
			PM	131.9	10.63	134.3	12.64	125.9	5.63	125.9	5.66	126.6	6.17	126.1	5.75
MT	-1	9.1	LM	10.1	11.22	12.0	31.36	13.2	45.35	13.3	45.82	10.4	14.54	12.8	41.20
			PM	13.9	53.16	16.6	82.16	9.0	-1.20	18.0	98.30	14.1	55.05	17.5	91.90
CT	0.1	7.2	LM	7.5	3.99	8.2	14.21	10.8	50.12	10.2	41.01	5.6	-22.49	7.2	0.00
			PM	10.3	43.28	11.4	58.44	7.3	2.06	13.8	91.85	7.6	5.12	9.8	36.49
Method				LM	PM	LM	PM	LM	PM	LM	PM	LM	PM	LM	PM
Max abs. error (%)				11.22	53.16	31.36	82.16	50.12	14.23	45.82	98.30	22.49	55.05	41.20	91.90
RMS error (%)				7.14	24.91	13.55	36.14	24.54	5.72	22.47	47.91	11.65	20.73	15.71	35.46

Table A.2. High-cycle fatigue strength predictions ($N_f=10^7$) for 42CrMo4+QT incorporating elastic-plastic stress redistribution at crack and notch tip.

Sample	R	Exp.	Method	Crossland		Sines		Fatemi-Socie		Findley		Carpinteri		MWCM	
				Pred.	Err (%)	Pred.	Err (%)	Pred.	Err (%)	Pred.	Err (%)	Pred.	Err (%)	Pred.	Err (%)
Plain	-1	390	LM	379.9	-2.59	382.6	-1.89	372.8	-4.42	389.3	-0.17	384.9	-1.30	388.4	-0.41
			PM	380.5	-2.42	382.7	-1.88	372.6	-4.46	390.6	0.15	385.0	-1.27	389.4	-0.15
	0.1	337	LM	337.9	0.28	337.6	0.18	338.7	0.50	337.1	0.02	337.7	0.21	337.2	0.05
			PM	337.8	0.25	337.6	0.17	338.8	0.54	336.9	-0.02	337.7	0.21	337.1	0.02
Sharp	-1	87.5	LM	88.2	0.82	88.2	0.84	89.2	1.92	87.6	0.10	88.1	0.71	87.7	0.22
			PM	88.2	0.75	88.2	0.82	89.1	1.79	87.4	-0.09	88.0	0.61	87.6	0.07
	0.1	80.5	LM	79.6	-1.06	79.8	-0.88	78.5	-2.52	80.4	-0.13	79.6	-1.13	80.3	-0.29
			PM	79.8	-0.92	79.8	-0.81	78.4	-2.56	80.6	0.11	79.6	-1.06	80.4	-0.10
Blunt	-1	162.7	LM	155.4	-4.49	162.0	-0.45	147.2	-9.52	148.9	-8.50	147.5	-9.32	148.6	-8.67
			PM	155.7	-4.30	162.0	-0.41	147.2	-9.56	149.5	-8.11	147.7	-9.20	149.1	-8.34
	0.1	119.2	LM	134.6	12.92	137.9	15.68	130.9	9.80	131.8	10.59	132.2	10.88	132.0	10.71
			PM	134.7	13.04	137.9	15.73	130.9	9.81	132.2	10.86	132.4	11.08	132.3	10.98
MT	-1	9.1	LM	8.8	-2.87	6.8	-25.18	10.0	9.47	11.3	23.78	9.4	3.43	10.6	16.61
			PM	9.1	11.00	7.4	-18.66	7.2	-20.40	14.3	57.11	10.9	20.30	13.4	47.46
CT	0.1	7.2	LM	7.4	2.70	5.3	-26.62	8.1	12.80	9.3	29.10	5.5	-24.16	7.3	1.80
			PM	7.2	8.74	5.7	-20.55	6.1	-15.87	10.5	45.20	5.2	-27.49	4.6	-35.43
Method				LM	PM	LM	PM	LM	PM	LM	PM	LM	PM	LM	PM
Max abs. error (%)				12.92	21.37	26.62	20.55	12.80	20.40	29.10	57.11	24.16	27.49	16.61	47.46
RMS error (%)				5.14	11.66	14.11	11.31	7.66	10.52	14.13	26.19	10.03	13.13	7.66	21.50

Table A.3. High-cycle fatigue strength predictions ($N_f=10^7$) for 7075-T6 assuming linear-elastic stress distribution.

Sample	R	Exp.	Method	Crossland		Sines		Fatemi-Socie		Findley		Carpinteri		MWCM	
				Pred.	Err (%)	Pred.	Err (%)	Pred.	Err (%)	Pred.	Err (%)	Pred.	Err (%)	Pred.	Err (%)
Plain	-1	160.3	LM	160.5	0.11	159.9	-0.23	163.0	1.68	161.6	0.84	160.6	0.22	159.9	-0.25
			PM	160.4	0.07	159.9	-0.24	163.5	1.99	161.6	0.82	160.6	0.17	159.8	-0.30
	0.1	116.6	LM	115.7	-0.79	118.5	1.63	112.2	-3.78	109.4	-6.14	114.2	-2.02	119.0	2.12
			PM	116.0	-0.53	118.6	1.72	112.8	-3.25	109.5	-6.06	114.6	-1.69	119.6	2.61
Sharp	-1	44.9	LM	44.7	-0.31	45.1	0.47	42.3	-5.70	43.5	-2.96	44.5	-0.89	45.0	0.22
			PM	44.8	-0.20	45.1	0.48	42.3	-5.78	43.6	-2.90	44.6	-0.69	45.0	0.21
	0.1	27.6	LM	27.7	0.29	27.5	-0.46	29.0	5.12	28.3	2.36	27.9	0.91	27.5	-0.41
			PM	27.7	0.18	27.5	-0.48	29.0	5.23	28.2	2.32	27.8	0.76	27.5	-0.49
Blunt	-1	63.5	LM	63.3	-0.30	68.4	7.70	63.1	-0.60	63.2	-0.43	63.6	0.17	63.5	-0.04
			PM	62.4	-1.70	68.0	7.10	62.7	-1.25	62.7	-1.34	62.9	-0.91	62.7	-1.24
	0.1	45.5	LM	41.5	-8.77	44.6	-2.04	43.4	-4.63	42.4	-6.90	43.8	-3.85	45.4	-0.14
			PM	41.2	-9.56	44.4	-2.34	43.2	-5.01	42.0	-7.60	43.6	-4.26	45.3	-0.34
MT	-1	4.2	LM	4.3	3.33	8.8	109.50	5.5	31.96	5.6	34.05	4.6	9.29	2.2	-47.25
			PM	5.7	34.52	11.9	182.28	7.3	74.89	7.5	78.10	6.1	44.76	3.1	-25.86
CT	0.1	2.5	LM	2.2	-11.60	2.4	-5.83	3.8	50.45	3.0	21.60	2.2	-13.20	-12.4	-597.47
			PM	2.9	15.60	3.2	27.27	5.0	99.63	4.0	61.60	2.9	14.80	-15.9	-734.68
Method				LM	PM	LM	PM	LM	PM	LM	PM	LM	PM	LM	PM
Max abs. error (%)				11.60	34.52	109.50	182.28	50.45	99.63	34.05	78.10	13.20	44.76	597.47	734.68
RMS error (%)				5.29	13.83	38.88	65.22	21.40	44.21	14.69	35.36	5.93	16.75	211.90	259.91

Figures

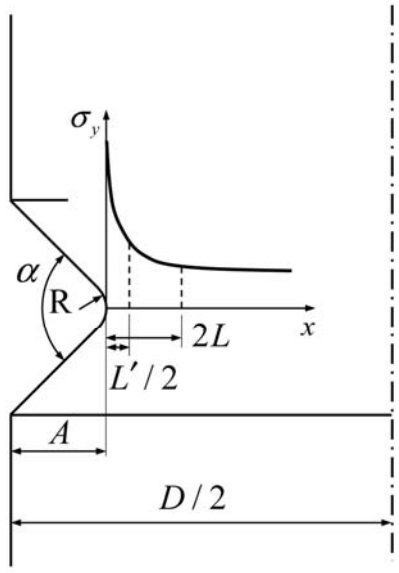

Fig. 1. Schematic illustration of the axisymmetric V-notched sample geometry. The coordinate *x* lies on the sample symmetry plane and is centred at the notch tip. *L* and *L*' are the critical distance lengths according to LM and PM.

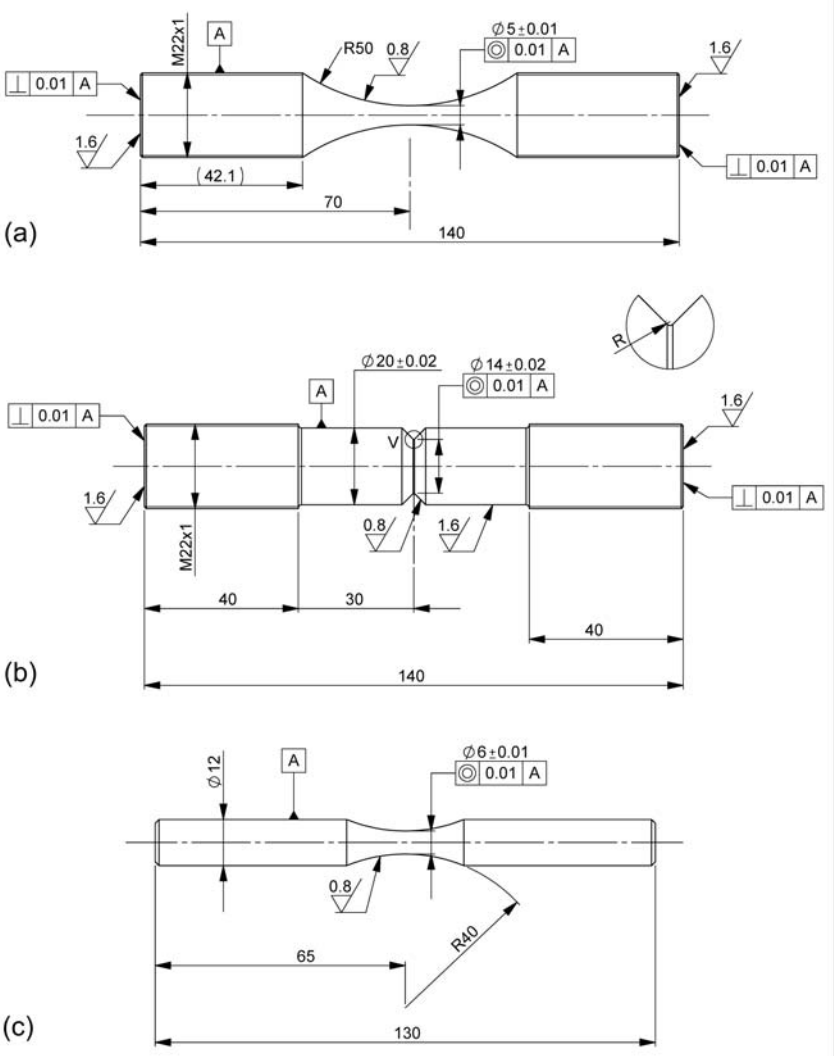

Fig. 2. Geometry of the specimens used in the present work. (a) plain, (b) notched samples for HCF tests. The notch root radius R is 0.2 mm for sharp and 1 mm for blunt notches. (c) Hourglass specimens for strain-controlled LCF tests. Dimensions are given in mm.

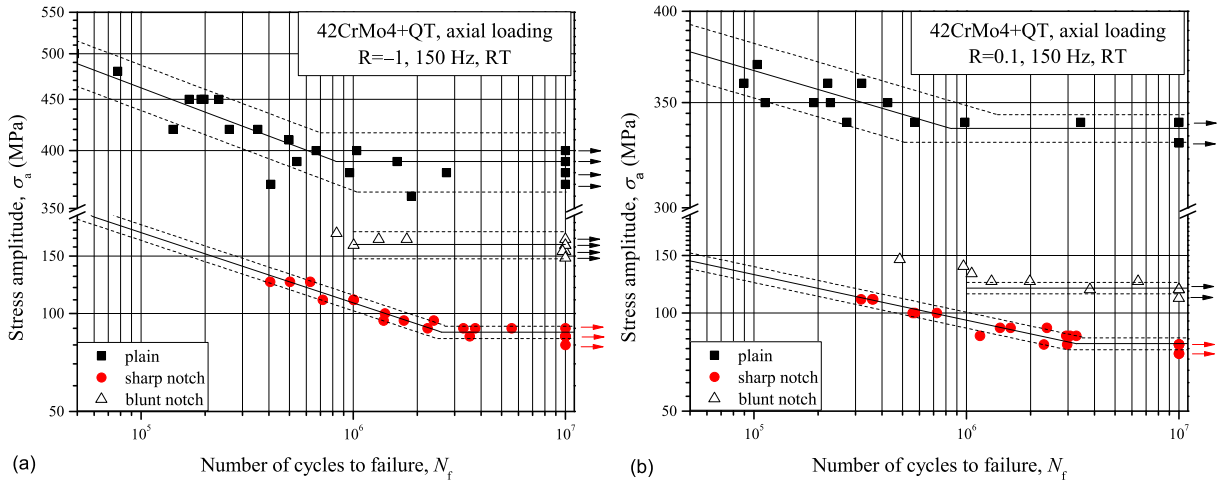

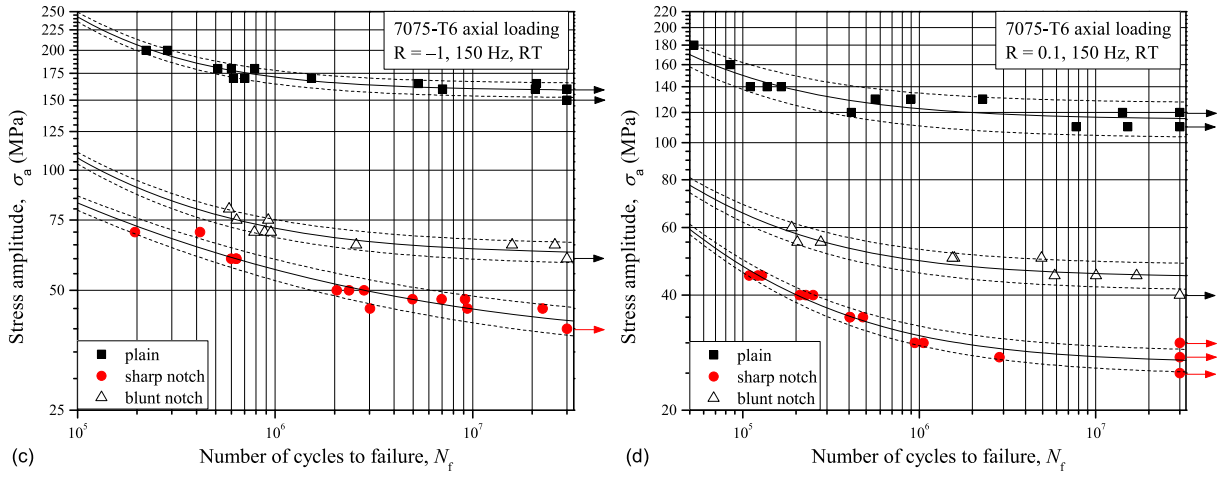

Fig. 3. Fatigue experimental data and fit curves for 42CrMo4+QT (a) load ratio R= −1, (b) R= 0.1, arrows indicate runouts at 10 × 10^6 cycles, and 7075-T6 (c) R= −1, (d) R= 0.1, arrows indicate runouts at 30 × 10^6 cycles. Dashed lines correspond to the fatigue strengths for the various specimens at 10% and 90% failure probabilities.

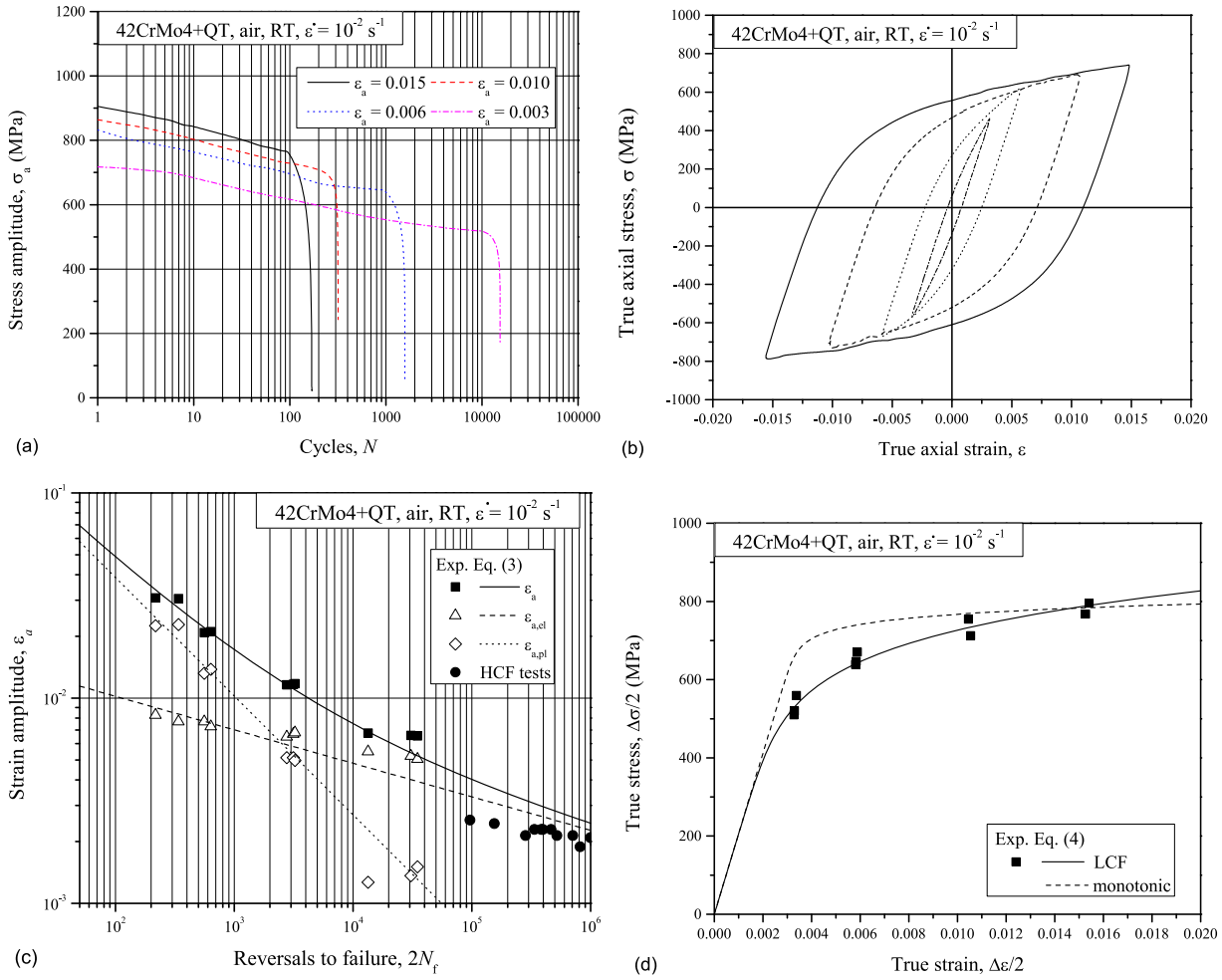

Fig. 4. Principal results of the LCF tests conducted on 42CrMo4+QT. (a) Evolution of the stress amplitude vs. number of strain cycles. (b) Stabilized hysteresis loops at half fatigue life. (c) Experimental data vs. Basquin and Coffin-Manson equations. (d) Comparison between monotonic and cyclic stress strain curve.

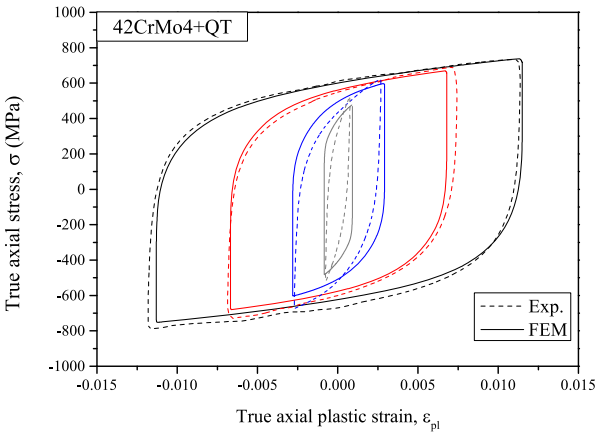

Fig. 5. Comparison between experimental and numerical plastic hysteresis loops. Solid lines are obtained by calibrating a three-submodel Chaboche kinematic hardening model to the loop of largest strain amplitude.

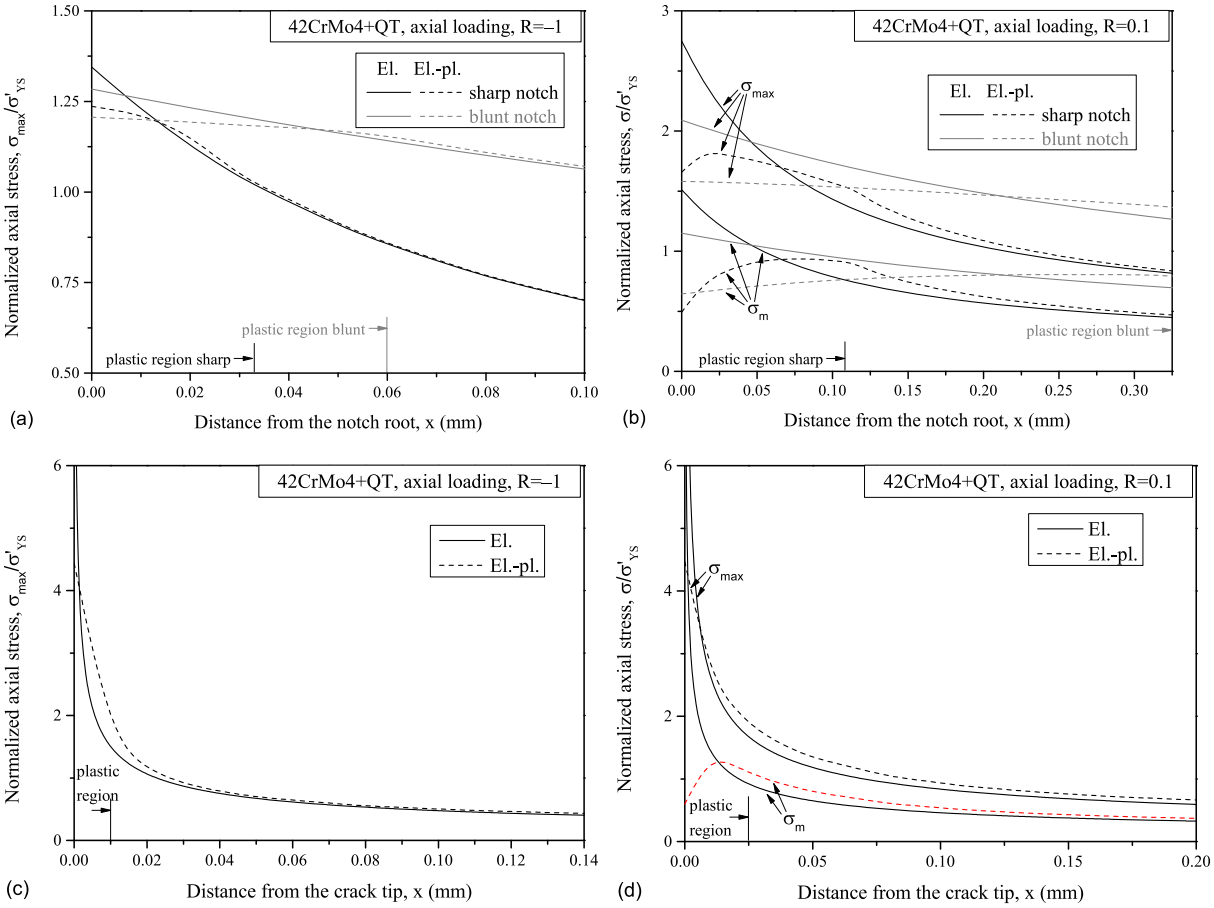

Fig. 6. Axial principal stress variation as a function of the distance (measured along the specimen axis of symmetric) from the notch/crack tip. The remote far field axial stress corresponds to the fatigue limit or crack threshold conditions for notched and cracked samples, respectively. Both maximum and minimum values are shown and normalized with respect to the cyclic yield stress σ'_{YS}. (a) and (b) notched samples, (c) and (d) crack tip stress field. (a) and (c) R = -1, (b) and (d) R = 0.1.

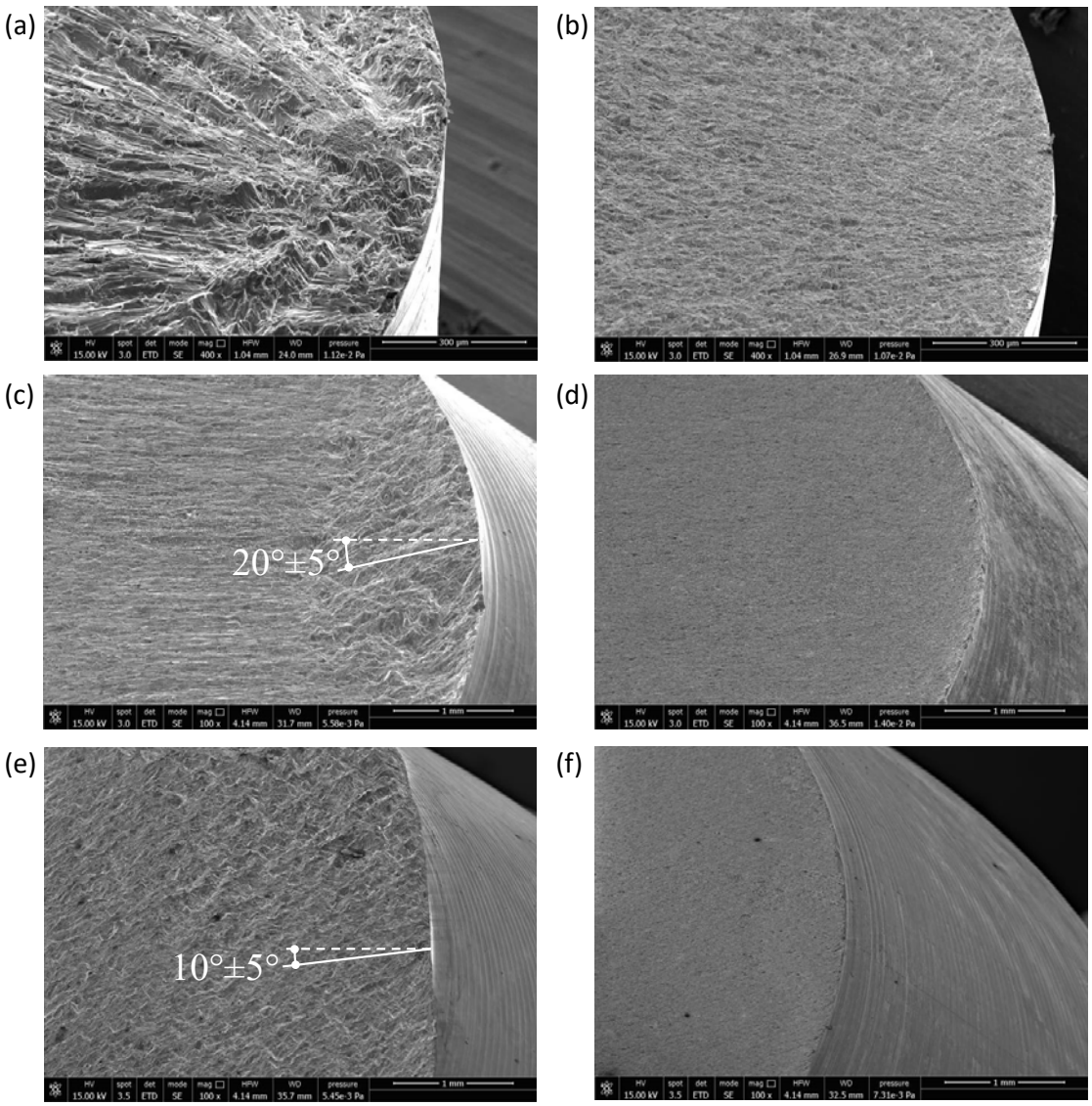

Fig. 7. SEM micrographs of the fracture surfaces of samples tested at load ratio R = 0.1: (a)-(c)-(e) aluminium alloy 7075-T6, (b)-(d)-(f) steel 42CrMo4+QT; (a)-(b) Plain specimens, (c)-(d) Blunt specimens, (e)-(f) Sharp specimens. (a) σ_a = 120 MPa, $N_f = 1.42 \times 10^7$, (b) σ_a = 340 MPa, $N_f = 3.44 \times 10^6$, (c) σ_a = 50 MPa, $N_f = 1.54 \times 10^6$, (d) σ_a = 125 MPa, $N_f = 6.42 \times 10^6$, (e) σ_a = 27.5 MPa, $N_f = 2.85 \times 10^6$, (f) σ_a = 85 MPa, $N_f = 3.28 \times 10^6$

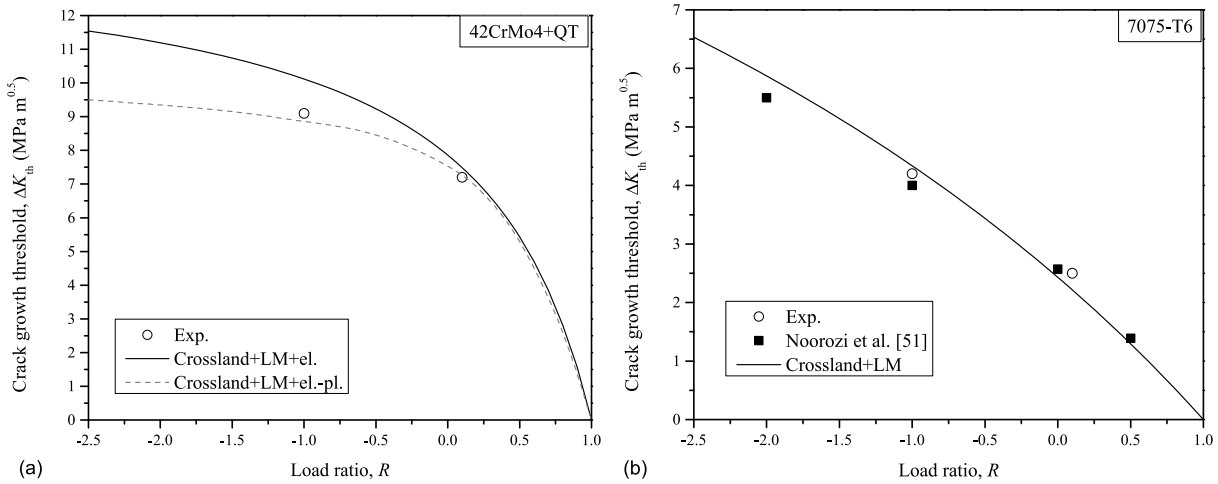

Fig. 8. Application of Crossland criterion in combination to LM for the prediction of the threshold conditions of long cracks as a function of the load ratio. (a) 42CrMo4+QT, (b) 7075-T6.

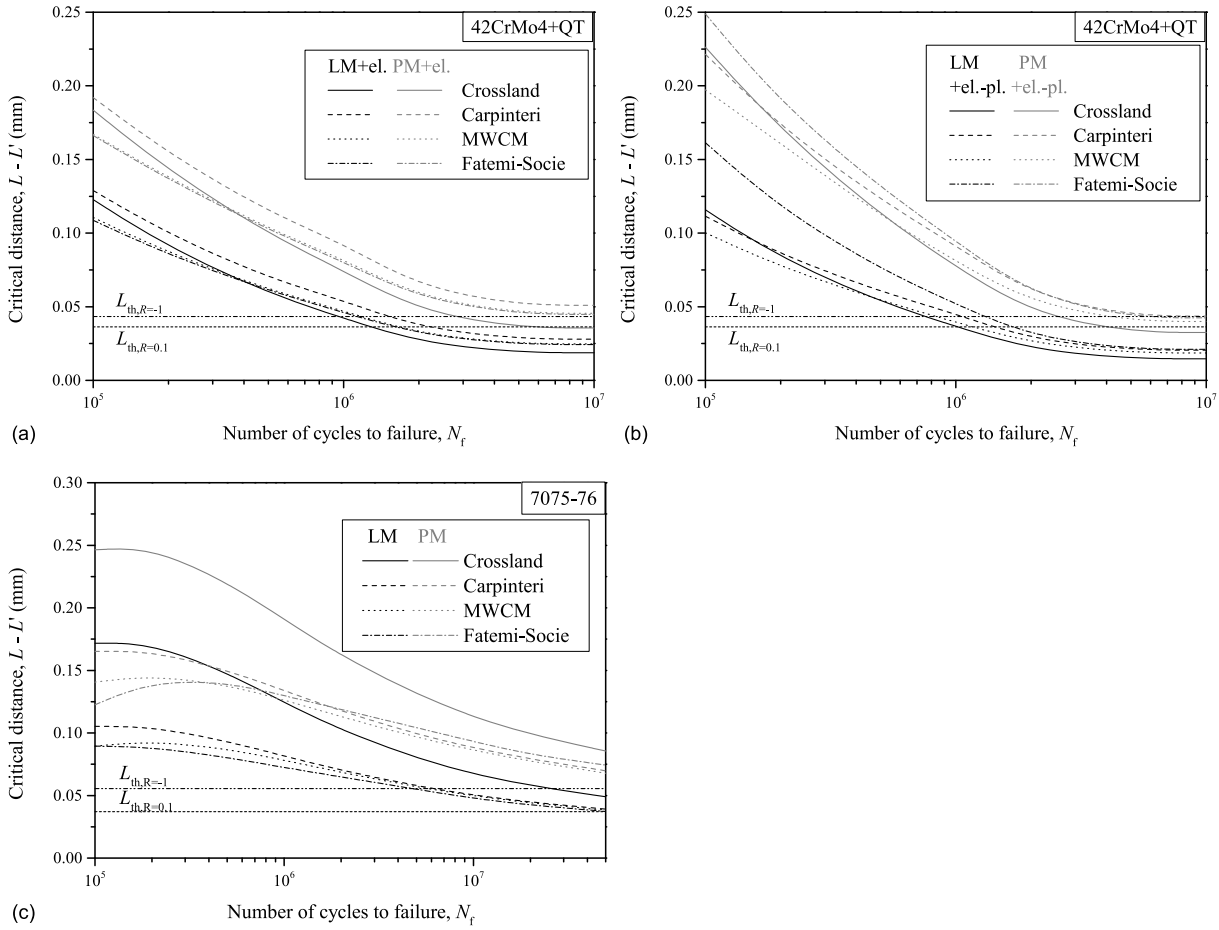

Fig. 9. Variation of the critical distance lengths L and L' with the number of cycles to failure. (a) and (b) 42CrMo4+QT, (c) 7075-T6. In (a) and (c) linear-elastic stress distribution is considered, while in (b) elastic-plastic stress redistribution at the notch tip is included.

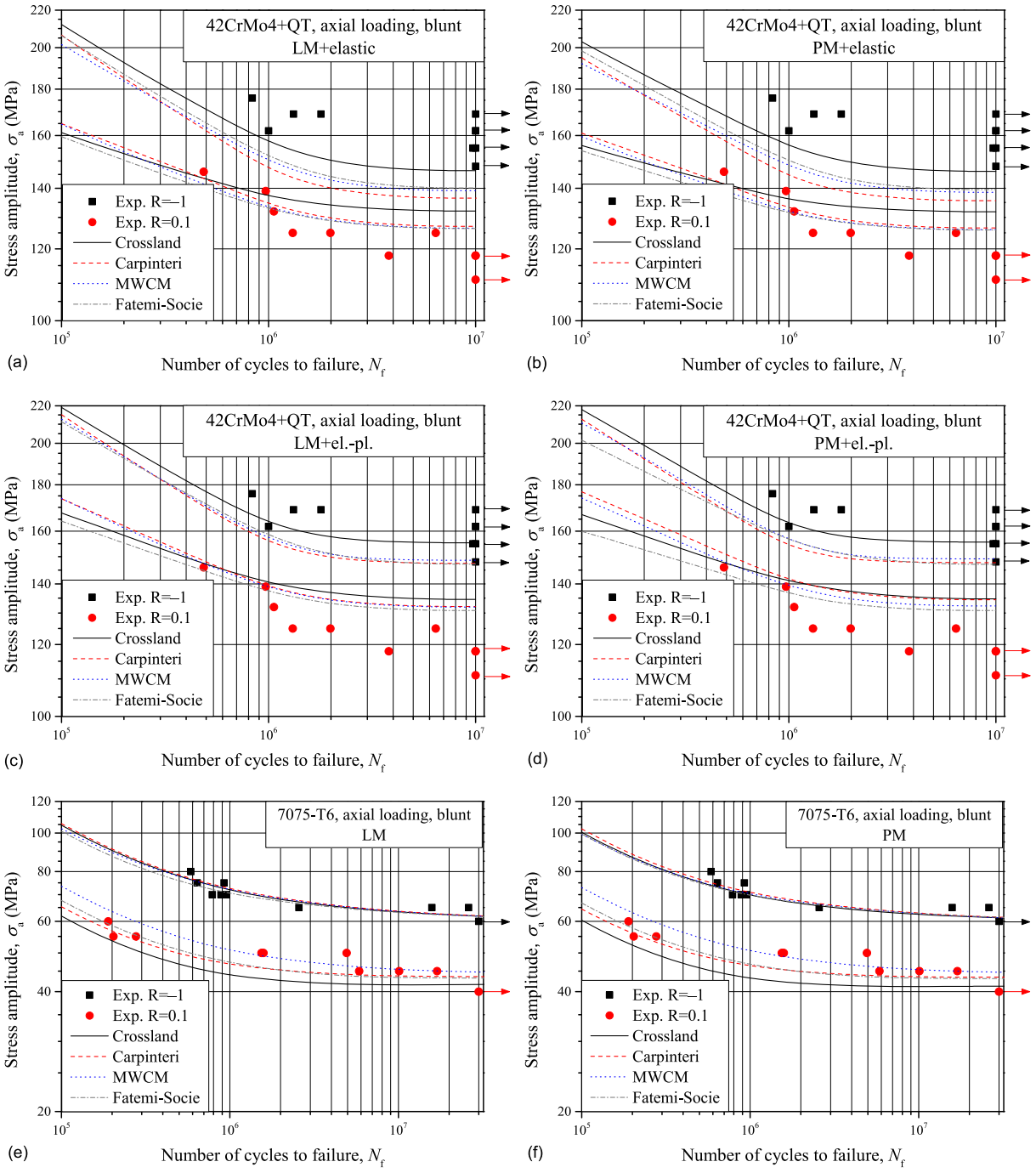

Fig. 10. Prediction of the fatigue curves of blunt-notched specimens using four different multiaxial fatigue criteria in combination with (a), (c), (e) LM and (b), (d), (f) PM. (a-d) 42CrMo4+QT, (e-f) 7075-T6. (a) and (b) are obtained under linear-elastic stress distribution, while (c) and (d) include elastic-plastic notch tip stress redistribution.